Lead-Halide Perovskites Meet Donor-Acceptor Charge-Transfer Complexes

Marchal, Nadège; Van Gompel, Wouter; Gélvez-Rueda, María C.; Vandewal, Koen; Van Hecke, Kristof; Boyen, Hans Gerd; Conings, Bert; Herckens, Roald; Maheshwari, Sudeep; Grozema, Ferdinand C.

DOI
10.1021/acs.chemmater.9b01289

Publication date
2019

Document Version
Accepted author manuscript

Published in
Chemistry of Materials

Citation (APA)
Marchal, N., Van Gompel, W., Gélvez-Rueda, M. C., Vandewal, K., Van Hecke, K., Boyen, H. G., Conings, B., Herckens, R., Maheshwari, S., & Grozema, F. C. (2019). Lead-Halide Perovskites Meet Donor-Acceptor Charge-Transfer Complexes. *Chemistry of Materials*, *31*(17), 6880-6888. https://doi.org/10.1021/acs.chemmater.9b01289

Lead-halide perovskites meet donor-acceptor charge-transfer complexes

Nadège Marchal*,[1], Wouter Van Gompel[2], María C. Gélvez-Rueda[3], Koen Vandewal[5], Kristof Van Hecke[4], Hans-Gerd Boyen[5], Bert Conings[5], Roald Herckens[2], Sudeep Maheshwari[3], Laurence Lutsen[6], Claudio Quarti[1], Ferdinand C. Grozema[3], Dirk Vanderzande[2], David Beljonne[1]

[1] Laboratory for Chemistry of Novel Materials, University of Mons, Place du Parc, 20, B-7000 Mons, Belgium

[2] Hasselt University, Institute for Materials Research (IMO-IMOMEC), Hybrid Materials Design (HyMaD), Martelarenlaan 42, B-3500 Hasselt, Belgium

[3] Optoelectronic Materials Section, Department of Chemical Engineering, Delft University of Technology, Van der Maasweg 9, 2629 HZ Delft, The Netherlands

[4] Ghent University, Department of Chemistry, XStruct, Krijgslaan 281-S3, B-9000 Ghent, Belgium

[5] Hasselt University, Institute for Materials Research, (IMO-IMOMEC) Wetenschapspark 1, 3590 Diepenbeek, Belgium

[6] IMEC, Associated Laboratory IMOMEC, Wetenschapspark 1, B-3590 Diepenbeek, Belgium

Lead halide perovskites, Charge-Transfer complexes, Hybrid materials, DFT electronic structure

ABSTRACT: Low-dimensional lead halide hybrid perovskites are nowadays in the spotlight because of their improved stability and extensive chemical flexibility compared to their 3D perovskite counterparts, the current challenge being to design functionalized organic cations. Here, we report on the synthesis and full characterization of a perovskite-like hybrid where the 1D lead iodide layout is patterned with a donor-acceptor charge transfer complex (CTC) between pyrene and tetracyaniquinodimethane. By combining multiple structural analysis and spectroscopic techniques with *ab initio* modelling, we show that the electronic, optical and charge-transport properties of the hybrid materials are dominated by the organic CTC, with the inorganic backbone primarily acting as a template for the organization of the donor and acceptor molecules. Interestingly, time-resolved microwave conductivity (TRMC) measurements show an enhanced photocurrent generation in the 1D hybrid compared to the pure organic charge-transfer salt, likely associated with transient localization of the holes on the lead-iodide octahedra. This observation is line with the close energy resonance between the valence crystal orbitals of the lead-iodide lattice and the frontier occupied molecular orbitals of pyrene predicted by the DFT calculations. Therefore, it paves the way toward the design of new hybrid low-dimensionality perovskites offering a synergic combination of organic and inorganic functionalities.

INTRODUCTION

Lead halide hybrid perovskites have received significant attention over the last decade as semiconductor materials, namely for photovoltaic applications.[1-3] These materials possess a peculiar crystalline structure with a ABX_3 stoichiometry, where X is an halogen atom (I^-, Br^-, Cl^-), B an inorganic cation (Pb^{2+}, Sn^{2+}...) and A an organic cation ($CH_3NH_3^+$, $NH_2CHNH_2^+$). The structure consists in a three-dimensional network of corner-shared BX_6 octahedra with A cations located in the cavities of this framework.

While these 3D hybrid materials can be easily prepared from solutions of precursors and display impressive opto-electronic properties, e.g. with a certified power conversion efficiency of 23.7%[4], they suffer from degradation issues mainly associated with ionic diffusion in the inorganic network[5]. This has driven the community to design low-dimensional hybrid perovskites that, in addition to higher stability, offer structural versatility, prompting their use as active components in a wide range of optoelectronic applications.[6-13] Indeed, the constraint that the organic cation should obey a strict geometrical rule to fit in the cavities created by the inorganic octahedral network in the 3D case is alleviated when going to lower-dimensionality materials[14]. As a result, by properly tuning the nature of the organic cation and/or the synthesis protocol, it is now possible to engineer lead halide organic-inorganic hybrids where the inorganic framework formed by the PbI_6^{4-} octahedra span the full dimensionality range from 3D to 2D, 1D or 0D.[6-13]

Layered perovskite materials containing alkylammonium cations have been scrutinized in the past. While the study of these provides useful insight into the effects of dielectric confinement[15, 16] and local lattice distortions[17-20], the range of tenability offered by inert organic cations is limited. An attractive strategy to convey additional functionalities to the resulting hybrid materials is to replace the inert cations by electroactive organic conjugated molecules. Organic charge-transfer complexes (CTCs) have distinct optical fingerprints[21] and have been extensively studied over the last 50 years for their interesting properties, including ambipolar charge transport,

metallicity, photoconductivity and ferroelectricity.[21-25] In this context, we have recently shown that organic donor-acceptor charge-transfer complexes can be combined with 2D layered hybrid perovskites.[26] 2D perovskites with a general structural formula $(D\text{-}C_nH_{2n}\text{-}NH_3{:}A\ 1{:}1)_2PbI_4$ were obtained, where D is a donor molecule (e.g. pyrene) and A an acceptor molecule (e.g. tetracyanoquinodimethane, TCNQ). The acceptors are incorporated into the organic layer through the formation of charge-transfer complexes with donors that are tethered to the inorganic framework via an alkylammonium chain. Unfortunately, we were at that time not able to resolve single-crystal structures of these 2D hybrids, preventing detailed structure-property relationships to be unraveled.

Here, we report on our ongoing efforts towards the synthesis of hybrid materials, in which the organic component contributes to the charge transport, combining in a synergic way the complementary properties of their organic and inorganic components. More specifically, we synthesized novel 1D hybrids composed of wires of face-sharing PbI_6^{4-} octahedra separated by bilayers containing the CTCs, with a stoichiometry of $(D\text{-}C_nH_{2n}\text{-}NH_3{:}A\ 1{:}1)PbI_3$ (Fig. 1a). The crystal structures of the mixed organic-inorganic hybrid and has have been elucidated using single-crystal X-ray diffraction (XRD) (Fig.1b) and was found to be monoclinic. The powder X-ray diffraction (PXRD) pattern of the bulk sample of crystal compared well with the simulated pattern from single-crystal XRD (Figure S1). The crystal structure of the pyrene:TCNQ organic CTC was taken from the literature, a representation is shown in Fig. 1c.[27] The experimental PXRD pattern of our grown pyrene:TCNQ crystals matched well with the simulated pattern based on the crystal structure from literature (Fig.2). The 1D hybrid perovskites show very good thermal stability in ambient atmosphere, as assessed based on temperature-controlled XRD measurements (Figure S9 and S10). In addition to structural information, XPS valence band and TRMC measurements, combined with DFT computational investigations, provide detailed information about the electronic structure and the charge generation and transport properties of these novel hybrid materials. Altogether, our combined theory-experiment study conveys the message that: (i) the inorganic lattice mostly acts as a template for the local organization of the organic conjugated molecules, and (ii) the close energy resonance between the occupied levels on the inorganic and organic parts improves photoinduced charge generation.

RESULTS & DISCUSSION

Electronic structure and optical properties

Optical absorption spectra measured by photothermal deflection spectroscopy for the 1D hybrid perovskite and the organic CTC crystals are reported in Fig. 2 (see also Absorption Spectra Fig. S5 and S6). While the shape of the two spectra is similar, pointing to the similar nature of the involved electronic excited states, a clear blue shift by ~0.3eV of the sharp absorption onset is observed when going from the Pyr:TCNQ pure organic crystal to the 1D hybrid perovskite. Such a spectral displacement might originate from various (combined) contributions, namely a different molecular packing of the CTC or direct full or partial involvement of the lead halide inorganic skeleton through hybridization with the organic chromophores.

We resort to DFT electronic structure calculations to address the origin of the observed differences in electronic structure and optical properties between the organic and the hybrid crystals. As a first step, an in-depth study was performed to analyze the sensitivity of the results against details of the modeling methodology. It has indeed been widely documented that the inclusion of spin-orbit coupling (SOC) effects and an accurate treatment of electronic exchange and correlation energy are key to a quantitative description of the electronic structure of lead halide perovskites[28-29]. Details about the modeling approach are provided in Supporting Information (Table 1, Fig. S7). In a nutshell, after realizing that SOC does not influence the lowest unoccupied energy levels (localized on the TCNQ acceptors), we selected (unless otherwise specified) plane-wave DFT calculations in combination with a hybrid functional (PBE0), as implemented in the Quantum Espresso package suite[30]. Using this methodology, we obtain an electronic bandgap of 1.93 eV for the 1D perovskite system, to be compared with 2.16 eV for the pure CTC crystal. While compared to the PDS data the theoretical values are expectedly blue shifted, namely by the exciton binding energy but also inherent errors associated with the choice of DFT functionals, the calculations do however correctly reproduce the observed spectral shift (~0.23eV calculated against ~0.3eV measured) between the two crystals.

Turning to the electronic structure energy diagrams displayed in Figure 3a, we find from the analysis of the partial Density of states (DOS) that the band-edge levels in the 1D hybrid perovskite are fully confined on the organic part, namely with the conduction band-edge (CBE) dominated by TCNQ empty orbitals and the valence band-edge (VBE) governed by Pyrene occupied orbitals. It is important to stress, however, that the lead-iodide inorganic skeleton contributes with occupied crystalline orbitals that are located in close energy proximity (within ~0.1 eV) to the VBE – in contrast, the corresponding PbI unoccupied crystalline orbitals are located at significantly higher energies than the CBE. In addition, inspection of the partial DOS reveals no or very limited hybridization between the organic molecular and inorganic crystalline orbitals, which would materialize through the presence of a partial contribution of lead and iodine atoms at the VBE (and CBE) energy. In view of the small energy difference, this absence of wavefunction mixing must originate from a very weak electronic coupling matrix element, likely resulting from the poor electronic contact between the inorganic scaffold and the conjugated chromophores. Looking retrospectively at the optical absorption data, we thus rule out hybridization as a mechanism for the observed blue shift and rather invoke a reorganization of the donor and acceptor molecules templated by the inorganic layout. This is consistent with the (slight) change in the ground-state charge transfer density when going from the organic CT salt (with an effective charge per TCNQ molecule calculated to be ~0.15 |e| using a Bader charge analysis[31] reported in Supporting information Table S2) to the lead halide CT hybrid (where the charge per TCNQ amounts to ~0.21 |e|). We further note that the electronic band gap between the lead halide only crystalline orbitals is close to 4eV at the level of theory

considered. This is much higher than the corresponding bandgaps calculated at the same level of theory for 2D lead halide perovskites, highlighting the important role of dimensionality on the electronic structure of these materials.

Fig.3b displays both the predicted full (and partial) SOC-corrected DOS together with the simulated XPS spectrum, where relative intensities have been obtained through weighting the density of states by the relative photoionization cross sections of the involved valence electrons. While this approach should be considered with caution (as delocalized band states are obviously distinct from their contributing atomic orbitals), it explains the fact that occupied molecular orbitals arising from the organic components are hidden in the background noise of the XPS spectra because of their low ionization cross-sections. With this caveat, we can proceed with the comparison of the theoretical results to the experimental valence band electronic structure, here probed using XPS (as more bulk sensitive technique, information depth > 5 nm) instead of UPS (as more surface sensitive technique, information depth about 1 nm). The measured and predicted valence band spectra are dominated by the iodine atoms at low binding energies, while the SOC-split 5d orbitals of lead contribute a twin peak at higher binding energies (below -10eV). It is interesting to see that a better match with experiment regarding the absolute energies of the lead orbitals is obtained considering the bare (unscaled) DOS, which could indicate partial hybridization or simply reflect uncertainties in the computed orbital energies. Unfortunately, the limited spectral resolution and the low cross-sections of the sp2 carbon atoms from the pyrene molecules do not allow to ascertain the theoretical finding that the VBE is mostly sourced by the organic molecules. As demonstrated below, this is indirectly supported by charge transport measurements.

Charge transport properties

Table 1 reports the calculated effective masses along high-symmetry paths for: (i) the hybrid 1D organic-inorganic perovskite; (ii) the pure organic CT salt; and (iii) a hypothetical system built by removing all lead and iodine atoms from the crystal structure of the hybrid material and (to balance the charges) substituting the nitrogen atoms of the ammonium groups with carbons. This aims at mimicking a pure template effect where the inorganic lattice would not participate directly to the transport properties but eventually indirectly through a reorganization of the spatial rearrangement of the donor and acceptor molecules in comparison to the CT salt. As a matter of fact, in all relevant directions, the effective masses predicted by the DFT calculations are typical for organic molecular crystals with weak band dispersion. The differences observed between the hybrid and the organic crystal primarily stem from a template effect, as confirmed by comparing the relatively similar effective masses computed for the real hybrid and hypothetical structures. This template effect materializes mostly as differences in intermolecular distances along TCNQ and Pyrene molecular rows in the b direction for the CTC crystal and the corresponding c direction for the 1D hybrid perovskite, see Fig.1c. More specifically, there is a reduced herringbone angle, or similarly a smaller longitudinal molecular translation, between successive donor (acceptor) molecules in the hybrid structure. As a result, the electron effective masses along the high-mobility direction (c) are significantly smaller, especially for electrons, in the hybrid material with respect to the pure salt (for which b is the high-mobility direction), a difference that reflects the more substantial wavefunction overlap between the molecular orbitals in presence of the inorganic template. Yet, the absolute values of the effective masses remain relatively large for both holes and electrons, irrespective of the direction, hence we expect relatively poor charge transport mobility for both organic and hybrid crystals.

This is fully confirmed by Time-Resolved Micro-Conductivity (TRMC) measurements that probe the change in conductivity after excitation using high-frequency microwaves. In particular, we have performed Pulse-Radiolysis (PR) TRMC measurements to monitor the temperature-dependent mobility of free charge carriers in the two materials. The results plotted in Fig.4a show modest (10^{-3}-10^{-2} $cm^2V^{-1}s^{-1}$) and similar mobility values over a broad temperature range in the pure organic salt and in the organic-inorganic hybrid crystals. In addition, similar recombination dynamics of the charge carriers are obtained, see Supporting Information (Fig. S8 and S9).

To complement these studies, photoconductivity TRMC measurements have also been performed at different excitation wavelengths. In addition to providing insight into the recombination dynamics, the early spike in the time evolution of the photoconductivity signal measures the yield of photogenerated free electrons and holes. Exciting in the charge-transfer band results in a larger photoconductivity signal for the 1D hybrid perovskite compared to the organic salt, see Fig. 4b. Besides, the recombination lifetime of the charge carriers is longer. As no appreciable difference in charge carrier mobility could be measured from the PR-TRMC experiments discussed above, we therefore conclude that the higher photoconductivity signal in the hybrid film must be caused by a higher yield of mobile free charge carriers. We speculate that the larger fraction of photogenerated free charge carriers in the hybrid material is related to transient localization of the holes on the inorganic lattice facilitated by the close energy spacing between the occupied inorganic crystalline and organic molecular occupied orbitals, *vide supra*.

CONCLUSIONS

We have reported on the synthesis of a novel, thermally stable, 1D hybrid material where charge-transfer complexes between molecular donors and acceptors act as charge compensating organic cations, thus offering new functionalities to the resulting hybrid materials. These have been extensively characterized using a battery of structural analysis and spectroscopic techniques in combination with molecular modelling. Our investigations show that most of the electronic and optical properties of the CTC salt are retained, with the inorganic lattice primarily acting as a template for the spatial arrangement of the molecular chromophores. As a result, modest charge transport properties with charge carrier mobility not exceeding 10^{-2} $cm^2V^{-1}s^{-1}$ have been obtained. However, a first indication pointing towards some coupling between the inorganic and organic manifolds in these mixed systems is the

increased photocurrent generation, likely favored by transient localization of the holes on the lead halide backbone. Moreover, the novel hybrids discussed in this article offer a high degree of potential tunability. As can be deduced from the general formula (D-C_nH_{2n}-NH_3:A 1:1)PbX_3, one could potentially change the core of the donor molecule (D), the alkyl chain length of the donor molecule (C_nH_{2n}), the acceptor molecule (A) and the halide (X). All of these changes are suspected to have a (more or less significant) degree of influence on the optical and electronic properties of these hybrids. Therefore, the applicability of this type of hybrids can potentially be extended by using donor:acceptor combinations with superior charge transport properties compared to pyrene:TCNQ. Charge-transfer complexes can also exhibit a variety of electronic or magnetic properties and it would be interesting to determine how their inclusion into an inorganic scaffold influences these.

EXPERIMENTAL METHODS

Chemicals and reagents. 7,7,8,8-Tetracyanoquinodimethane (TCNQ, > 98.0%) was bought from TCI. Potassium phthalimide salt (95%) were obtained from Fluorochem. Lead iodide (PbI_2, 99.999%) was obtained from Lumtec. 1-Pyrenebutyric acid (95%) was purchased from Combi-Blocks, Inc. Lithium aluminium hydride ($LiAlH_4$, 95%), carbon tetrabromide (CBr_4, 98%), potassium carbonate (K_2CO_3, 99+%), magnesium sulfate ($MgSO_4$, 99%), ammonium chloride (NH_4Cl, 99+%), triphenylphosphine (Ph_3P, 99%), pyrene (98%), hydrazine monohydrate (65%) and hydriodic acid (57 wt.% aqueous solution) were bought from Fisher Scientific. All chemicals were used without further purification. The dry dimethylformamide (DMF) that was used to make the precursor solutions, and dry tetrahydrofuran (THF) which was used for the reactions, was obtained from our in-house solvent-purification system (MBRAUN SPS-800). All other solvents were purchased from Fisher Scientific.

The $PyrC_4NH_3I$ salt was synthesized as detailed in a previous publication.[9]

Single crystal growth. The single crystals of ($PyrC_4NH_3$:TCNQ 1:1)PbI_3 were grown using an antisolvent vapor-assisted crystallization approach[32] in which the components are dissolved together in a good solvent (γ-butyrolactone; GBL) and dichloromethane (DCM) anti-solvent slowly diffuses into the GBL solution. Specifically, $PyrC_4NH_3I$, TCNQ and PbI_2 were dissolved together in gamma-butyrolactone by stirring at 50 °C for 15 min (Table 2). The precursor solution was filtered through a syringe filter (0.45 μm). The precursor solution (0.5 ml) was transferred to a small glass vial. The small vial (5 ml volume) was capped off with aluminum foil. A small hole was made in the aluminum foil. The small vial with the aluminum foil was put in a larger glass vial (20 ml volume). A small amount of dichloromethane (2 ml) was injected in the gap between the two flasks and the larger flask was capped off with a plastic cap and parafilm. The vials were left undisturbed at room temperature. After 1 week black crystals suitable for single-crystal X-ray diffraction were harvested. These crystals were washed three times with dry dichloromethane and were subsequently dried under reduced pressure at room temperature.

Table 2. Concentration of components used for the single crystal synthesis of ($PyrC_4$:TCNQ 1:1)PbI_3.

$PyrC_4NH_3I$ concentration (mol/l)	TCNQ concentration (mol/l)	PbI_2 concentration (mol/l)
0.108	0.108	0.108

The crystals of the organic CTC pyrene:TCNQ were grown by dissolving equimolar amounts of pyrene and TCNQ (Table 3) in tetrahydrofuran (THF) by stirring at 40°C until full dissolution. The solution was allowed to cool down to room temperature and was filtered through a syringe filter (0.45 μm). Crystals were obtained by evaporation of the THF at room temperature.

Table 3. Concentration of components used for the crystals of pyrene:TCNQ.

Pyrene concentration (mol/l)	TCNQ concentration (mol/l)
0.025	0.025

Thin film deposition. Stoichiometric amounts of $PyrC_4NH_3I$, TCNQ and PbI_2 were dissolved in dry DMF by stirring at 50 °C for 30 min (Table 4). The precursor solution was filtered through a syringe filter (0.45 μm) before use.

Quartz substrates were cleaned through consecutive sonication steps in a series of solvents (detergent water, deionized water, acetone, isopropanol) for 15 min each, followed by a UV-ozone treatment for 15 min. Films were obtained by drop-casting (~ 30 μl on a 2.5 cm x 2.5 cm substrate) on a quartz substrate. The films were annealed at 110 °C for 15 min.

Table 4. Concentration of components used for thin film deposition of ($PyrC_4$:TCNQ 1:1)PbI_3.

$PyrC_4NH_3I$ concentration (mol/l)	TCNQ concentration (mol/l)	PbI_2 concentration (mol/l)
0.3	0.3	0.3

Characterization. **X-ray diffraction** measurements were performed at room temperature in ambient air on a Bruker D8 Discover diffractometer with CuK_α radiation. Temperature-controlled XRD measurements were performed on the same instrument with a temperature cell, under nitrogen flow.

Photothermal deflection spectroscopy measurements. Photothermal Deflection Spectroscopy (PDS) was performed using a home-built set-up: chopped (4.1 Hz) monochromatic light from a 100 W Quartz-Tungsten-Halogen lamp is focused onto the crystal. The crystal is glued onto a quartz substrate with inert transparent glue (ethyl-2-cyanoacylate). Substrate and sample are immersed in perfluorohexane (C6F14, 3M Fluorinert FC-72). A HeNe (633 nm) probe laser passes through

the deflection medium and grazes the surface of the sample. Absorption of monochromatic light results in a slight heating of sample and deflection medium. The latter has a strongly temperature dependent refractive index, resulting in deflection of the probe laser, of which the amplitude is detected by a position-sensitive Si detector, connected to a Stanford Research Systems SR830 lock-in amplifier. The incident light intensity is measured at the same time by a pyro-electric detector. The PDS signal is obtained by dividing the deflection signal by the signal coming from the pyroelectric detector, and is for weakly emissive samples proportional to the absorption spectrum.[33]

Valence band spectroscopy was carried out on a commercial electron spectrometer (PHI-5600LS), equipped with a smallspot X-ray source providing monochromatized Al-k radiation (photon energy 1486.6 eV). During the XPS measurements, an overall energy resolution (photons and electrons) of 0.36 eV full-width-at-half-max (FWHM) was applied.

Pulse-radiolysis microwave conductivity measurements. High energy pulse microwave conductivity measurements were performed on micrometer crystals (~45 mg) placed in a Polyether ether ketone (PEEK) holder. The PEEK block with the sample is placed inside a rectangular waveguide cell (chemically inert gold-plated copper). The cell is contained in a cryostat in which the temperature can be varied between 123K and 473K. The irradiation intensity was varied between pulse lengths of 5 ns and 50 ns (charge carrier concentrations ~$2x10^{16}$ cm^{-3} to $2x10^{17}$ cm^{-3}) for each temperature at a frequency of 31 GHz. The frequency scan (28-38 GHz) fits were measured at a pulse length of 20 ns (~$9.9x10^{16}$ cm^{-3}).[34]

Photo-conductivity measurements. Laser induced time-resolved microwave conductivity (TRMC) measurements were performed on thin films deposited on quartz substrates and placed in a sealed resonant cavity inside a nitrogen-filled glovebox. Photoconductivity TRMC measurements quantify the change in conductivity [microwave (8-9 GHz) power] upon pulsed excitation (repetition rate 10 Hz) due to free mobile charge carriers. The change of microwave power is related to the change in conductivity before and during the photo-conductance measurements, the samples were kept in an inert nitrogen environment to prevent degradation by exposure to moisture.[35]

THEORETICAL METHODS

Electronic properties. Density functional theory calculations[36-40] with periodic boundary conditions have been performed with the Quantum Espresso suite program[30] for the electronic properties (and Bader analysis[31]) using a planewave/ pseudopotential formalism. We adopted a norm-conserving pseudopotential, with a cutoff of 40 Ry for the expansion of the wave function, and a correction for the van der Waals interactions (Grimme DFT-D2 method[41]). Different functionals (GGA and Hybrids) were applied: PBE[42], PBE0 and HSE. In the case of the PBE functional, we also performed the same calculations with and without a spin-orbit correction. We kept the same k-points mesh for all PBE calculations, 4 x 3 x 2 for the organic crystal (Pyr:TCNQ) and 4 x 1 x 4 for the 1D perovskite. When using hybrid functionals, the calculations were limited at the gamma point of the first brillouin zone, because of the calculation costs.

Charge transport properties. Effective masses calculations have also been performed with Quantum Espresso at the PBE level. We instead resorted to the CRYSTAL suite program (CRYSTAL14[43, 44], CRYSTAL17[45, 46]) for effective mass calculations using hybrid functionals, namely the PBE0 functional, as these are not implemented in Quantum Espresso. For consistency between the two set of results, we paid attention to keep the same cell parameters, the same number of atoms explicitly taken into account and the same k-points mesh for the single point calculations.

AUTHOR INFORMATION

Corresponding Author

* Email: Nadege.MARCHAL@umons.ac.be

Author Contributions

The manuscript was written through contributions of all authors. All authors have given approval to the final version of the manuscript.

Notes

The authors declare no competing financial interest.

ACKNOWLEDGMENT

The FWO is acknowledged for the funding of research. W.T.M.V.G. is an SB PhD fellow at FWO (Number 1S17516N), R. H. is a special research fund (BOF) doctoral (PhD) student at UHasselt/IMO. K. V. H. thanks the Hercules Foundation (Project AUGE/11/029 "3D-SPACE: 3D Structural Platform Aiming for Chemical Excellence") and the special research fund (BOF) – Ugent (Project 01N03217) for funding. The work has been carried out in the context of the solliance network (www.solliance.eu), from which UHasselt and TUDelft are members. Additionally UHasselt is a partners in the Energyville Consortium (http://www.energyville.be/about-energyville). The research leading to these results in the Delft University of Technology has received funding from the Auropean Research Council Horizon 2020 ERC Grant Agreement no.648433.
The work from the University of Mons was supported by a 50-50 PhD funding for N.M. from the University of Mons, by the Interuniversity Attraction Pole program of the Belgian Referal Science Policy Office (PAI 6/27) and FNRS-F.R.S. Computational resources have been provided by the Consortium des Equipements de Calcul Intensif (CECI), funded by the Fonds de la Recherche Scientifique de Belgique (F.R.S.-FNRS) under Grant No. 2.5020.1 and by the Walloon Region. C.Q. and D.B. are FNRS postdoctoral researcher and research director, respectively.
KVH thanks the Hercules Foundation (project AUGE/11/029 "3D-SPACE: 3D Structural Platform Aiming for Chemical Excellence") and the Special Research Fund (BOF) – UGent (project 01N03217) for funding. Bart Ruttens and Jan D'Haen (IMO-IMOMEC) are acknowledged for PXRD measurements.

ASSOCIATED CONTENT

The Supporting Information is available free of charge on the ACS Publications website.

Experimental details of the single crystal XRD measurement, Powder XRD, Comparison between 2D and 1D hybrids containing CTCs, Absorption Spectra, Theoretical methodological study, Bader analysis, Pulse-Radiolysis TRMC, Thermal stability of the hybrid. (PDF)

REFERENCES

(1) Shi, Z.; Jayatissa, A. Perovskites-Based Solar Cells: A Review of Recent Progress, Materials and Processing Methods. *Materials (Basel).* **2018**, *11* (5), 729.

(2) Koijama, A.; Teshima, K.; Shirai, Y.; Miyasaka, T. Organometal Halide Perovskites as Visible-Light Sensitizers for Photovoltaic Cells. *J. Am. Chem. Soc.* **2009**, 131, 6050-6051.

(3) Stranks, S. D.; Snaith, H. J., Metal-halide perovskites for photovoltaic and light-emitting device. *Nat. Nanotechnol.* **2015**, 10, (5), 391-402.

(4) NREL's "Best Research-Cell Efficiencies " Chart, https://www.nrel.gov/pv/assets/pdfs/pv-efficiency-chart.20181221.pdf.

(5) Meng, L., You, J., Yang, Y., Addressing the stability issue of perovskite solar cells for commercial applications, *Nat. Commun.* **2018**, 9, 5265.

(6) Grancini, G., Roldàn-Carmona, C., Zimmermann, I., Mosconi, E., Lee, X., Martineau, D., Narbey, S., Oswald, F., De Angelis, F., Gratzel, M., et al. One Year Stable Perovskite Solar Cells by 2D/3D Interface Engineering. *Nat. Commun.* **2017**, 8, 15684

(6) Saidaminov, M. I.; Mohammed, O. F.; Bakr, O. M. Low-Dimensional-Networked Metal Halide Perovskites: The Next Big Thing. *ACS Energy Lett.* **2017**, *2* (4), 889–896.

(7) Lin, H.; Zhou, C.; Tian, Y.; Siegrist, T.; Ma, B. Low-Dimensional Organometal Halide Perovskites. *ACS Energy Lett.* **2018**, *3* (1), 54–62.

(8) Etgar, L. The Merit of Perovskite's Dimensionality; Can This Replace the 3D Halide Perovskite? *Energy Environ. Sci.* **2018**, *11* (2), 234–242.

(9) Van Gompel, W. T. M.; Herckens, R.; Van Hecke, K.; Ruttens, B.; D'Haen, J.; Lutsen, L.; Vanderzande, D. Low-dimensional Hybrid Perovskites Containing an Organic Cation with an Extended Conjugated System: Tuning the Excitonic Absorption Features. *ChemNanoMat* **2018**, 5, (3), 323-327.

(10) Mao, L.; Stoumpos, C. C.; Kanatzidis, M. G. Two-Dimensional Hybrid Halide Perovskites: Principles and Promises. *J. Am. Chem. Soc.* **2019**, *141* (3), 1171–1190.

(12) Grancini, G.; Nazeeruddin, M. K. Dimensional Tailoring of Hybrid Perovskites for Photovoltaics. *Nat. Rev. Mater.* **2019**, *4* (1), 4–22.

(13) Herckens, R.; Van Gompel, W. T. M.; Song, W. Y.; Gelvez-Rueda, M. C.; Maufort, A.; Ruttens, B.; D'Haen, J.; Grozema, F. C.; Aernouts, T.; Lutsen, L.; Vanderzande, D., Multi- layered hybrid perovskites templated with carbazole derivatives: optical properties, enhanced moisture stability and solar cell characteristics. *Journal of Materials Chemistry A* **2018**, 6, (45), 22899-22908.

(14) Amat, A., Mosconi, E., Ronca, E., Quarti, C., Umari, P., Nazeeruddin, M. K., Graetzel, M., De Angelis, F. Cation-Induced Band Gap Tuning in Organohalide Perovskites: Interplay of Spin-Orbit Coupling and Octahedral Tilting. *Nano Lett.*, **2014**, 14, 3608-3616

(15) Even, J.; Pedesseau, L.; Katan, C. Understanding Quantum Confinement of Charge Carriers in Layered 2D Hybrid Perovskites. *ChemPhysChem* **2014**, 15, 3733−3741

(16) Sapori, D.; Kepenekian, M.; Pedesseau, L.; Katan, C.; Even, J. Quantum Confinement and Dielectric Profiles of Colloidal Nanoplatelets of Halide Inorganic and Hybrid Organic-Inorganic Perovskites. *Nanoscale* **2016**, 8, 6369−6378.

(17) Quarti, C., Marchal, N., Beljonne D., Tuning the Optoelectronic Properties of Two-Dimensional Hybrid Perovskite Semiconductors with Alkyl Chain Spacers. *J. Phys. Chem. Lett.*, **2018**, 9(12), pp 3416-3424

(18) Gan, L., Li, J., Fang, Z., He, H., Ye, Z., Effects of Organic Cation Length on Exciton Recombination in Two-Dimensional Layered Lead Iodide Hybrid Perovskite Crystals. *J. Phys. Chem. Lett.*, **2017**, 8, 5177-5183

(19) Traore, B.; Pedesseau, L.; Assam, L.; Che, X.; Blancon, J.-C.; Tsai, H.; Nie, W.; Stoumpos, C. C.; Kanatzidis, M. G.; Tretiak, S.; et al. Composite Nature of Layered Hybrid Perovskites: Assessment on Quantum and Dielectric Confinements and Band Alignment. *ACS Nano* **2018**, 12, 3321−3332.

(20) Motta, C.; El-Mellouhi, F.; Kais, S.; Tabet, N.; Alharbi, F.; Sanvito, S. Revealing Hte Role of Organic Cations in Hybrid Halide Perovskite CH3NH3PbI3. *Nat. Commun.* **2015**, 6, 7026.

(21) Jiang, H.; Hu, P.; Ye, J.; Zhang, K. K.; Long, Y.; Hu, W.; Kloc, C. Tuning of the Degree of Charge Transfer and the Electronic Properties in Organic Binary Compounds by Crystal Engineering: A Perspective. *J. Mater. Chem. C* **2018**, *6*, 1884–1902.

(22) Zhang, J.; Xu, W.; Sheng, P.; Zhao, G.; Zhu, D. Organic Donor–Acceptor Complexes as Novel Organic Semiconductors. *Acc. Chem. Res.* **2017**, *50* (7), 1654–1662.

(23) Sun, L.; Zhu, W.; Yang, F.; Li, B.; Ren, X.; Zhang, X.; Hu, W. Molecular Cocrystals: Design, Charge-Transfer and Optoelectronic Functionality. *Phys. Chem. Chem. Phys.* **2018**, *20* (9), 6009–6023.

(24) Zhang, J.; Jin, J.; Xu, H.; Zhang, Q.; Huang, W. Recent Progress on Organic Donor–acceptor Complexes as Active Elements in Organic Field-Effect Transistors. *J. Mater. Chem. C* **2018**, *6* (14), 3485–3498.

(25) Lingyun, Z., et al. Electronic Properties of Mixed-Stark Organic Charge-Transfer Crystals. *J. Phys. Chem. C*. **2014**, 118, 14150-14156

(26) Van Gompel, W. T. M.; Herckens, R.; Van Hecke, K.; Ruttens, B.; D'Haen, J.; Lutsen, L.; Vanderzande, D., Towards 2D layered hybrid perovskites with enhanced functionality: introducing charge-transfer complexes via self-assembly. *Chem Commun.* **2019**, 55, (17), 2481-2484.

(27) Do browolski, M. A.; Garbarino, G.; Mezouar, M.; Ciesielski, A.; Cyrański, M. K. Structural Diversities of Charge Transfer Organic Complexes. Focus on Benzenoid Hydrocarbons and 7,7,8,8-Tetracyanoquinodimethane. *CrystEngComm* **2014**, *16* (3), 415-429

(28) Umari, P.; Mosconi, E.; De Angelis, F. Relativistic GW Calculations on CH3NH3PbI3 and CH3NH3SnI3 Perovskites for Solar Cell Applications. Sci. Rep. 2015, 4, 4467.

(29) Even, J.; Pedesseau, L.; Jancu, J.-M.; Katan, C. Importance of Spin−Orbit Coupling in Hybrid Organic/Inorganic Perovskites for Photovoltaic Applications. *J. Phys. Chem. Lett.* **2013**, 4, 2999-3005

(30) Giannozzi, P., et al., Quantum Espresso: a modular and open-source software project for quantum simulations of materials, *Journal of Physics: Condensed Matter* **2009**, 21, 395502

(31) Skùlason, E., Bader Analysis: Calculating the charge on individual atoms in molecules & crystals, *Presentation in PDF*

(32) Shi, D.; Adinolfi, V.; Comin, R.; Yuan, M.; Alarousu, E.; Buin, A.; Chen, Y.; Hoogland, S.; Rothenberger, A.; Katsiev, K.; et al. Low Trap-State Density and Long Carrier Diffusion in Organolead Trihalide Perovskite Single Crystals. *Science (80-.).* **2015**, *347* (6221), 519–522.

(33) Jackson, W. B., Amer, N. M., Boccara, A. C., Fournier, D. Photothermal deflection spectroscopy and detections. *Applied optics*, **1981**, 20(8), 1333-1344.

(34) Warman, J. M., De Haas, M. P., Dicker, G., Grozema, F. C., Piris, J., Debije, M. G. Charge Mobilities in Organic Semiconducting Materials Determined by Pulse-Radiolysis Time-Resolved Microwave Conductivity:Pi-Bond-Conjugated Polymers Versus Pi-Pi-Stacked Discotics. *Chem. Mater.* **2004**, 16, 4600-4609

(35) Savenije, T.J., Ferguson, A.J., Kopidakis, N., Rumbles, G. Revealing the Dynamics of Charge Carriers in Polymer: Fullerene Blends Using Photoinduced Time-Resolved

Microwave Conductivity. *J. Phys. Chem. C.* **2013**, 117(46), 24085-24103.

(36) Jensen, F., Introduction to computational chemistry, *John Wiley & Sonc, Inc*. **1999**

(37) Koch, W., Holthausen, M.C., A Chemist's Guide to Density Functional Theory, *Wiley-VCH*, second edition, **2001**

(38) Yu, H. S., et al., Perspective:Kohn-Sham density functional theory descending a staircase, *The Journal of Chemical Physics*, **2016**, 145, 130901

(39) Hohenberg, P.; Kohn, W. Inhomogeneous Electron Gas, *Phys. Rev.* **1964**, 136, B864-871

(40) Kohn, W.; Sham, L. J., Self-Consistent Equations Including Exchange and Correlation Effects, *Phys. Rev*. **1965**, 140, A1133-A1138

(41) Grimme, S., Semiempirical GGA-type Density Functional Constructed with a Long-Range Dispersion Correction, *J. Comput. Chem.* **2006**, 27, 1787-1799

(42) Perdew, J.P., Burke, K., Ernzerhof, M., Generalized Gradient Approximation Made Simple, *Physical Review Letters* **1996**, 77(18), p.3865-3868.

(43) Dovesi, R., Orlando, R., Erba, A., Zicovich-Wilson, C. M., Civalleri, B., Maschio, L., Ferrabone, M., De La Pierre, M., D'Arco, P., Noel, Y., Causa, M., Rerat, M., Kirtman, B. *Int. J. Quantum. Chem*. **2014**, 114, 1287

(44) Dovesi, R., Saunder, V. R., Roetti, C., Orlando, R., Zicovich-Wilson, C. M., Pascale, F., Civalleri, B., Doll, K., Harrison, N. M., Bush, I., J., D'Arco, P., Llunell, M., Causà, M., Noël, Y. CRYSTAL14 User's Manual (University of Torino, Torino, 2014)

(45) Dovesi, R., Erba, A., Orlando, R., Zicovich-Wilson, C. M., Civalleri, B., Maschio, L., Rerat, M., Casassa, S., Baima, J., Salustro, S., Kirtman, B., *WIREs Comput. Mol. Sci.* **2018**, 8, e1360

(46) Dovesi, R., Saunder, V. R., Roetti, C., Orlando, R., Zicovich-Wilson, C. M., Pascale, F., Civalleri, B., Doll, K., Harrison, N. M., CRYSTAL17 User's Manual (University of Torino, Torino, 2017)

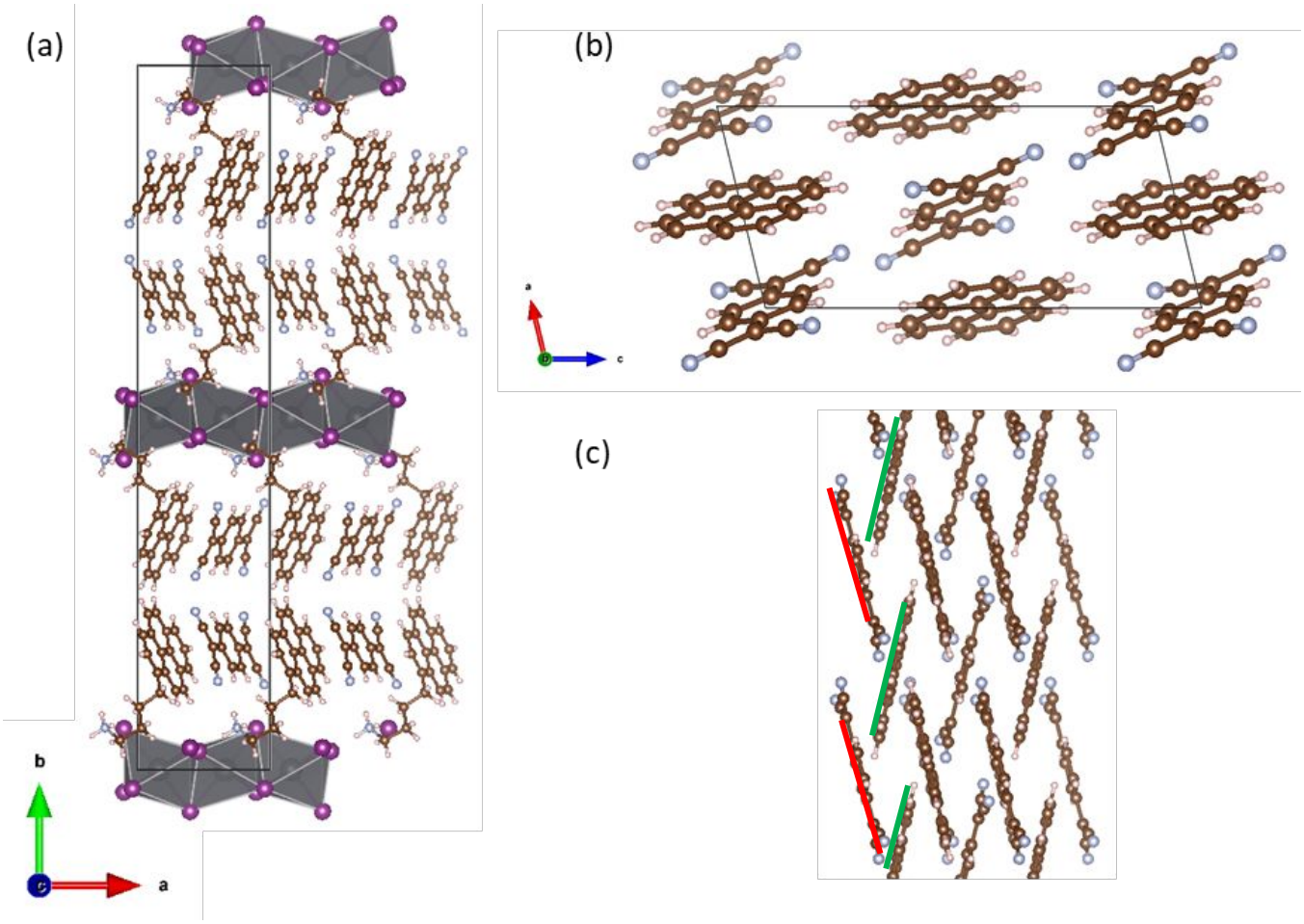

Figure 1. Crystal structures of the two investigated systems: (a) 1D hybrid ($PyrC_4NH_3$:TCNQ 1:1)PbI_3; the box shows the unit cell. Unit cell (b) and side view (c) of the molecular arrangement of the organic CTC (Pyr:TCNQ) crystal. [25]

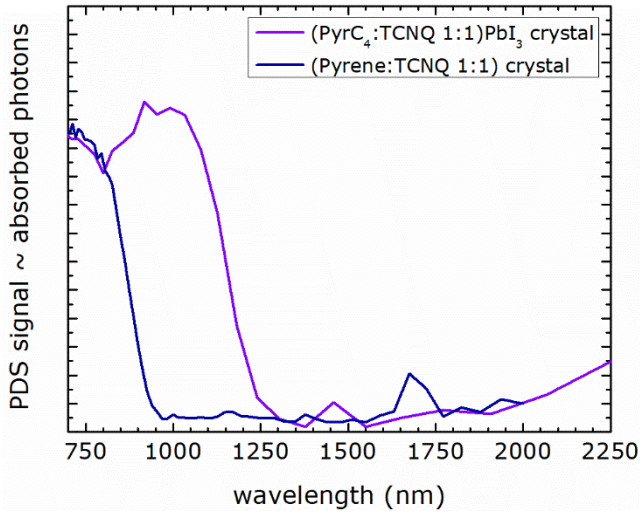

Figure 2. Optical absorption spectra of the 1D hybrid perovskite ($PyrC_4NH_3$:TCNQ 1:1)PbI_3 and CTC (Pyr:TCNQ) single crystals measured using Photothermal Deflection Spectroscopy.

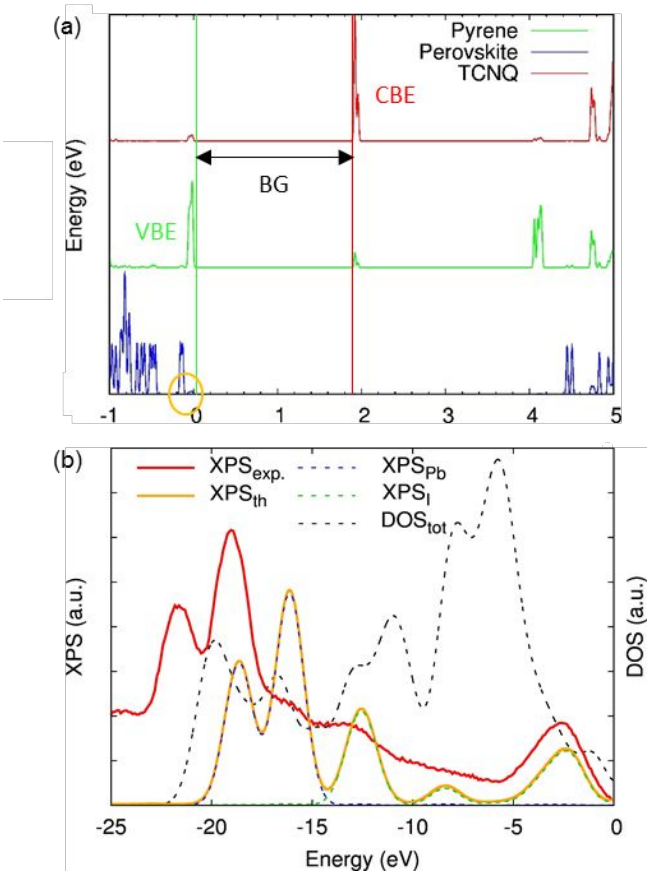

Figure 3. (a) Partial Density of States for the different components of the 1D hybrid perovskite ($PyrC_4NH_3$:TCNQ 1:1)PbI_3. The circled region indicates weak hybridization between the inorganic lattice and the CTC. VBE=Valence Band Edge; CBE=Conduction Band Edge; BG=Band Gap. (b) Comparison of the measured (in red) and calculated (in yellow) XPS spectra. Contributions from different elements scaled according to their photoionization cross-sections at the measured photon energy (1486.6 eV) are displayed as blue (for lead) and green (for iodine) dashed lines. The unscaled total DOS is shown by the dashed black line for comparison.

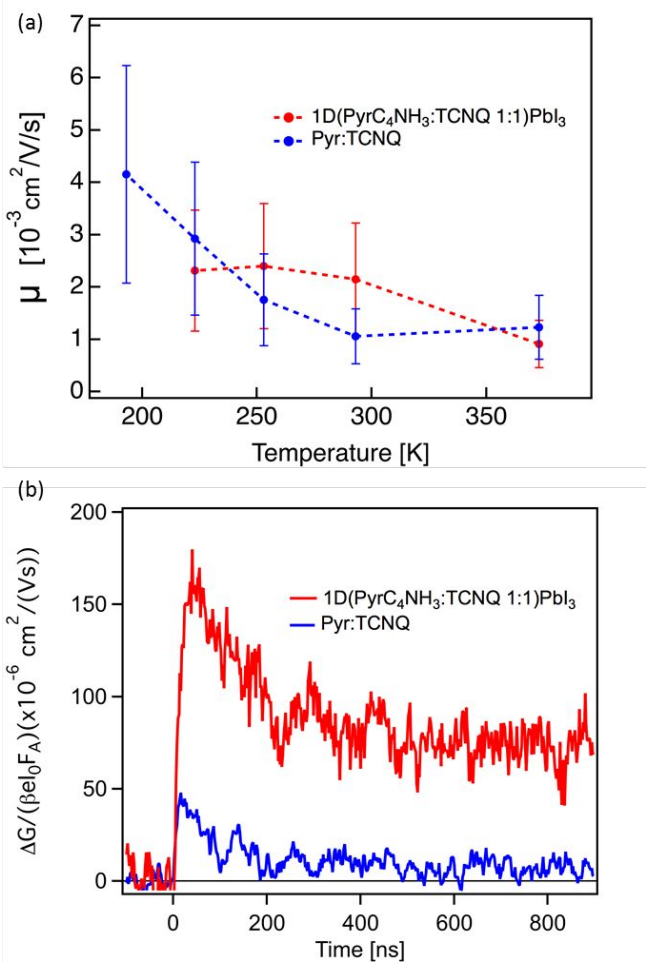

Figure 4. (a) Charge carrier mobility as a function of temperature for the two investigated systems: 1D hybrid perovskite ($PyrC_4NH_3$:TCNQ 1:1)PbI_3 and the CTC crystal (Pyr:TCNQ) (b) Photoconductivity TRMC measurements of 1D hybrid perovskite ($PyrC_4NH_3$:TCNQ 1:1)PbI_3 and the CTC crystal (Pyr:TCNQ) excited at the CT states.

Directions	***Organic CTC (Pyr:TCNQ 1:1)***		***1D CTC (Pyr:TCNQ 1:1)***		***1D perovskite - CTC (Pyr:TCNQ 1:1)PbI3***	
	m_{e-}	m_{h+}	m_{e-}	m_{h+}	m_{e-}	m_{h+}
(100)	*10.42*	*3.29*	*4.31*	∞	*4.63*	∞
(010)	***9.90***	***2.11***	∞	∞	∞	∞
(001)	*6.66*	*13.85*	*7.37*	*2.35*	***4.33***	***1.62***

Table 1. Effective masses of electrons and holes for the CTC crystal and the 1D hybrid perovskite ($PyrC_4NH_3$:TCNQ 1:1)PbI_3 crystals. We have also considered a hypothetical system (1D CTC) obtained by removing the inorganic layout from 1D hybrid perovskite structure in order to highlight the template effect.

Insert Table of Contents artwork here